Versatile and robust genome editing with *Streptococcus thermophilus* CRISPR1-Cas9

Daniel Agudelo[1], Sophie Carter[1], Minja Velimirovic[1], Alexis Duringer[1], Jean-François Rivest[1], Sébastien Levesque[1], Jeremy Loehr[1], Mathilde Mouchiroud[2], Denis Cyr[3], Paula J Waters[3], Mathieu Laplante[2,4], Sylvain Moineau[5,6,7], Adeline Goulet[8,9], and Yannick Doyon[1,4,*].

[1]Centre Hospitalier Universitaire de Québec Research Center - Université Laval, Québec, QC, G1V 4G2, Canada.

[2]Centre de recherche de l'Institut universitaire de cardiologie et de pneumologie de Québec (CRIUCPQ) - Université Laval, Québec, QC, G1V 4G5, Canada.

[3]Service de Génétique médicale, Département de Pédiatrie, Centre Hospitalier Universitaire de Sherbrooke (CHUS), Sherbrooke, QC, J1H 5N4, Canada.

[4]Université Laval Cancer Research Centre, Québec, QC, G1V 0A6, Canada.

[5]Département de biochimie, de microbiologie, et de bio-informatique, Faculté des sciences et de génie, Université Laval, Québec, QC, G1V 0A6, Canada.

[6]Groupe de recherche en écologie buccale, Faculté de médecine dentaire, Université Laval, Québec, QC, G1V 0A6, Canada.

[7]Félix d'Hérelle Reference Center for Bacterial Viruses, Faculté de médecine dentaire, Université Laval, Québec, QC, G1V 0A6, Canada.

[8]Architecture et Fonction des Macromolécules Biologiques, Centre National de la Recherche Scientifique (CNRS), Campus de Luminy, Case 932, 13288 Marseille Cedex 09, France

[9]Architecture et Fonction des Macromolécules Biologiques, Aix-Marseille Université, Campus de Luminy, Case 932, 13288 Marseille Cedex 09, France

[*]Corresponding author:
Yannick Doyon, Ph.D.
Centre de recherche du CHU de Québec – Université Laval
2705, boulevard Laurier, T-3-67
Québec, QC G1V 4G2
CANADA
Tel: 418-525-4444 ext. 46264
e-mail: Yannick.Doyon@crchudequebec.ulaval.ca

RUNNING TITLE

Orthologous St1Cas9 genome editing systems.

KEYWORDS

Genome editing, Base editing, Orthologous CRISPR-Cas9, *Streptococcus thermophilus* Cas9 (St1Cas9), Protospacer adjacent motif (PAM), Anti-CRISPR proteins (Acr), Adeno-associated virus (AAV), *In vivo* genome editing, Tyrosinemia.

ABSTRACT

Targeting definite genomic locations using CRISPR-Cas systems requires a set of enzymes with unique protospacer adjacent motif (PAM) compatibilities. To expand this repertoire, we engineered nucleases, cytosine base editors, and adenine base editors from the archetypal *Streptococcus thermophilus* CRISPR1-Cas9 (St1Cas9) system. We found that St1Cas9 strain variants enable targeting to five distinct A-rich PAMs and provide structural basis for their specificities. The small size of this ortholog enables expression of the holoenzyme from a single adeno-associated viral vector for *in vivo* editing applications. Delivery of St1Cas9 to the neonatal liver efficiently rewired metabolic pathways, leading to phenotypic rescue in a mouse model of hereditary tyrosinemia. These robust enzymes expand and complement current editing platforms available for tailoring mammalian genomes.

INTRODUCTION

Clustered regularly interspaced short palindromic repeats (CRISPR) and CRISPR-associated (Cas) proteins form a prokaryotic adaptive immune system and some of its components have been harnessed for robust genome editing (Komor et al. 2017). Type II-based editing tools rely on a large multidomain endonuclease, Cas9, guided to its DNA target by an engineered single-guide RNA (sgRNA) chimera (Jinek et al. 2012) (See (Koonin et al. 2017; Shmakov et al. 2017; Makarova et al. 2018) for a classification of CRISPR-Cas systems). The Cas9-sgRNA binary complex finds its target through recognition of a short sequence called the protospacer adjacent motif (PAM) and the subsequent base pairing between the guide RNA and DNA leads to a double-strand break (DSB) (Komor et al. 2017; Hille et al. 2018). While *Streptococcus pyogenes* (SpCas9) remains the most widely used Cas9 ortholog for genome engineering, the diversity of naturally occurring RNA-guided nucleases is astonishing (Shmakov et al. 2017). Hence, Cas9 enzymes from different microbial species can contribute to the expansion of the CRISPR toolset by increasing targeting density, improving activity and specificity as well as easing delivery (Esvelt et al. 2013; Komor et al. 2017).

In principle, engineering complementary CRISPR-Cas systems from distinct bacterial species should be relatively straightforward, as they have been minimized to only two components. However, many such enzymes were found inactive in human cells despite being accurately reprogrammed for DNA binding and cleavage *in vitro* (Ran et al. 2015; Zetsche et al. 2015; Chen et al. 2017a). Nevertheless, a striking example of the value of alternative Cas9 enzymes is the implementation of the type II-A Cas9 from

Staphylococcus aureus (SaCas9) for *in vivo* editing using a single recombinant adeno-associated virus (AAV) vector (Ran et al. 2015; Maeder et al. 2019). More recently, *Campylobacter jejuni* and *Neisseria meningitidis* Cas9s from the type II-C (Mir et al. 2018) CRISPR-Cas systems have been added to this repertoire (Kim et al. 2017; Ibraheim et al. 2018; Edraki et al. 2019). *In vivo* editing offers the possibility to generate phenotypes in animal models in order to better recapitulate the interactions between cell types and organs. In addition, it can be envisioned as a novel class of human therapeutics that enables precise molecular correction of genetic defects underlying diseases. Therefore, further development of robust and wide-ranging CRISPR-based technologies for *in vivo* editing may help to decipher disease mechanisms and offer novel therapeutic options (Lau and Suh 2017; Schneller et al. 2017).

Here we revisited the properties of *Streptococcus thermophilus* type II-A CRISPR1-Cas9, a model system central to the discovery of CRISPR and its function (Barrangou and Horvath 2017; Hille et al. 2018). We aimed to engineer potent RNA-guided nucleases and base editors with distinctive PAM sequences for both *in vitro* and *in vivo* applications.

RESULTS

Robust and potent DNA cleavage by St1Cas9 in human cells

While characterizing the interplay between St1Cas9 and anti-CRISPR proteins isolated from phages infecting *S. thermophilus* (Hynes et al. 2018) we noticed the substantial levels of editing achieved in human cells, an observation contrasting with previous

reports (Chari et al. 2015; Ran et al. 2015). We thus attempted to optimize its activity. First, we flanked the human codon-optimized ORF (Kleinstiver et al. 2015b) with nuclear localization signals (NLS) (Fig. 1A). Second, we customized the sgRNA sequence to maximize nuclease activity and tested our constructs at three endogenous loci (Fig. 1A,B; Supplemental Fig. S1A–F). The best performing sgRNA architecture (v1) was engineered by truncating the repeat:anti-repeat region (Briner et al. 2014) and substituting a wobble base pair present in the lower stem for a canonical Watson-Crick base pair (Fig. 1A). These modifications also markedly improved transcriptional activation using dSt1Cas9-VPR (Chavez et al. 2015) (Supplemental Fig. S2). This analysis revealed that high gene disruption rates could be obtained under standard conditions using St1Cas9 in human cells.

Functional PAM sequences for St1Cas9 LMD9 in mammalian cells

Cas9 orthologs rely on different PAMs as the first step in target recognition and the consensus PAM for St1Cas9 (LMD9 and DGCC7710 *S. thermophilus* strains that differ by only 2 aa within their N-terminus) was originally defined as NNAGAAW (where W is A or T) (Deveau et al. 2008). However, sequences closely related to the consensus can be functional in test tubes or when transplanted in *E. coli* for St1Cas9 LMD9, the strain variant first engineered for genome editing (Cong et al. 2013; Esvelt et al. 2013; Kleinstiver et al. 2015b; Leenay et al. 2016). We thus explored its PAM preference by targeting endogenous loci in human and mouse cells. This analysis revealed that St1Cas9 LMD9 functions efficiently at both NNAGAA and NNGGAA PAMs (Fig. 1C). While a C is tolerated at position 7, there is a trend for these guides to be less efficacious. This

bias was also observed in bacterial cells (Leenay et al. 2016). Thus, the functional core PAM sequence is constituted of four specific base pairs and defined as NNRGAA (where R is A or G). The optimal PAM sequence to regularly achieve high levels of editing is NNRGAAD (where D is A or G or T). The length of the nonconserved PAM linker (NN) has also been shown to be flexible and an extension from 2 to 3 bases can be tolerated in bacterial cells (Briner et al. 2014; Chen et al. 2014), but we failed to reproduce this observation in human cells suggesting a higher stringency of the system (Supplemental Fig. S1G). We also explored the impact of varying guide length on activity and observed no obvious correlation, confirming previous observations (Kleinstiver et al. 2015b) (Supplemental Fig. S1H). As 20bp guides are markedly less tolerant of mismatches than longer ones for SaCas9 (type II-A SaCas9 and St1Cas9 share 37% identity), we favor the use of 20bp guides (Tycko et al. 2018). Hence, the flexibility of PAM recognition by St1Cas9 LMD9 enhances its targeting capabilities. While recognition of an A-rich PAM may facilitate targeting A/T-rich regions of genomes, the targeting range of St1Cas9 in mammalian cells is less constrained than originally thought.

Engineering St1Cas9 variants to expand its targeting range

Although not formally defined as the PAM at the time, the presence of a degenerate consensus sequence situated downstream of protospacers has been observed in strains of *S. thermophilus* almost 15 years ago (Bolotin et al. 2005). For example, inferred consensus PAM sequences for St1Cas9 from strains CNRZ1066 and LMG13811 are NNACAA(W) and NNGYAA(A) (where Y is C or T), respectively (Bolotin et al. 2005). Accordingly, the CRISPR1-Cas system of *S. thermophilus* strain LMG13811 transplanted

in *E. coli* or reconstituted from purified components has been shown to target DNA using a NNGCAAA PAM (Chen et al. 2014).

At the protein level, the sequence of those St1Cas9 strain variants diverges mostly within the C-terminal wedge (WED) and PAM-interacting (PI) domains, implying that they have evolved to recognize distinct PAM sequences (Supplemental Fig. S3A,D). Since the PAM duplex is sandwiched between them (Fuchsbauer et al. 2019), we tested whether swapping the WED and PI domains of St1Cas9 LMD9 with the ones from LMG18311 and CNRZ1066 could reprogram PAM specificity (Fig. 2A). The same sgRNA architecture was used with all St1Cas9 variants for these experiments. While St1Cas9 LMD9 targeted NNAGAA and NNGGAA PAMs, the hybrid constructs targeted with high efficacy NNGCAA and NNACAA PAMs, respectively (Fig. 2A). We observed minimal levels of cross reactivity when swapping sgRNAs between nucleases, indicating that these variants have distinct PAM requirements for high cleavage efficacy (Fig. 2A). LMD9 and CNRZ1066-based variants recognized the non-cognate NNGCAA PAM with some sgRNAs, albeit cleavage efficacy was diminished (Fig. 2A).

Sequence database mining using the “Search for PAMs by ALignment Of Targets” (SPAMALOT) tool (Chatterjee et al. 2018) predicts that even more diversity exists within CRISPR1-StCas9 systems and two additional groups represented by strains TH1477 and MTH17CL396 potentially target NNGAAA and NNAAAA PAMs, respectively (Supplemental Fig. S3B). Using the strategy described above, we were able to construct highly active nucleases targeting NNGAAA and NNAAAA PAMs (Supplemental Fig.

S3C). These variants also displayed a high level of specificity for their cognate PAM despite differing by only 2 residues (see below; Supplemental Fig. S3C,D).

These data highlight the modularity inherent to Cas9 enzymes and a simple strategy to further expand the targeting range of St1Cas9s. Currently, this set of nucleases based on the St1Cas9 backbone can target five unique A-rich PAMs (LMD9; NNRGAA, LMG18311; NNGCAA, CNRZ1066; NNACAA, TH1477; NNGAAA, and MTH17CL396; NNAAAA). Tapping into the natural diversity found within *S. thermophilus* strains results in true reprograming towards a distinct PAM as opposed to relaxing specificity. In addition, despite their sequence and structural conservation (Nishimasu et al. 2015; Fuchsbauer et al. 2019) St1Cas9 variants could not cleave at SaCas9 PAMs (NNGRRT; where R is A or G) in human cells, further highlighting their specificity (Supplemental Fig. S4A–D). These orthologs also differ in their sensitivity to anti-CRISPR proteins as St1Cas9 is inhibited by both AcrIIA5 and AcrIIA6 while SaCas9 can only be blocked by AcrIIA5 (Supplemental Fig. S4E,F) (Hynes et al. 2018; Fuchsbauer et al. 2019; Garcia et al. 2019). This comparison between St1Cas9 and SaCas9 suggests that they function orthogonally and could be used in a combinatorial manner.

Structural basis for St1Cas9s PAM specificity

We recently determined the structure of St1Cas9 (DGCC7710) bound to its sgRNA and to a target DNA containing a PAM to an overall resolution of 3.3 Å using single particle cryo-electron microscopy (Fuchsbauer et al. 2019). In this structure, the 5'-GCAGAAA-3'-containing PAM duplex is formed by seven Watson-Crick base pairs, and

its major and minor grooves are sandwiched between the WED and PI domains. While the resolution of this structure prevents us from mapping all amino acid contacts with the PAM, the side chain of K1086 in the PI domain hydrogen bonds with the guanine at position 4 (NNA$\underline{G}_4$AA) (Fig. 2B). Accordingly, St1Cas9 variants predicted by SPAMALOT (Chatterjee et al. 2018) to specify a guanine at this position contain K1086 (Supplemental Fig. S3B,D). There is only one type of substitution at that position, where K1086 is replaced by I1086 (Supplemental Fig. S3D). This set of variants, which includes LMG18311 (NNG$\underline{C}_4$AA), CNRZ1066 (NNA$\underline{C}_4$AA), TH1477 (NNG$\underline{A}_4$AA), and MTH17CL396 (NNA$\underline{A}_4$AA) have lost the specificity for a guanine at position 4. At position 1084, the same type of analysis reveals that substitution of Q1084 for R1084 leads to the recognition of a guanine at position 3, as directly observed for LMG18311 (NN$\underline{G}_3$CAA) and TH1477 (NN$\underline{G}_3$AAA) (Fig. 2A; Supplemental Fig. S3C). Note that K1086 and R1084 are mutually exclusive and their co-occurrence would result in a steric clash (Supplemental Fig. S3D). In the structure of SaCas9 bound to 5'-TT$\underline{G}_3$AAT-3' PAM, the guanine at position 3 is recognized by R1015 (Nishimasu et al. 2015). Structural comparison reveals that SaCas9 R1015 and St1Cas9 Q1084 occupy the same position relative to their PAMs (Fig. 2C). In addition, SaCas9 R1015 is anchored via salt bridges to E993, a position equivalent to E1057 in St1Cas9 (Fig. 2C). Thus, St1Cas9 variants with R1084 likely recognize guanine at position 3 in an analogous manner as SaCas9 does. Finally, a distinct set of amino acids surrounding positions 1048-1052 likely specify an adenine at position 4 in some variants as it is the case for TH1477 (NNG$\underline{A}_4$AA), and MTH17CL396 (NNA$\underline{A}_4$AA) (Supplemental Fig. S3D). T1048 and M1049 are replaced by N1048 and D1049 in those St1Cas9 variants and are predicted to

occupy the same positions as N985 and N986 in SaCas9, the residues that specify purines at positions 4 and 5 in the $NNGR_4R_5T$ PAM (where R is A or G) (Nishimasu et al. 2015) (Fig. 2D; Supplemental Fig. S3D). Structural comparison predicts that N1048 could directly contact the adenine in position 4, and that N1048 and D1049 would contact the adenine in positions 4 and 5, potentially via water-mediated hydrogen bonds as observed in SaCas9 (Fig. 2D) (Nishimasu et al. 2015). Taken together, these observations provide a first glimpse at PAM recognition by St1Cas9 variants.

Broadening the targeting scope of base editors using St1Cas9 variants

DNA base editors comprise fusions between a catalytically impaired Cas nuclease and a base modification enzyme that operates on single-stranded DNA (ssDNA) (Rees and Liu 2018). Cytosine base editors (CBEs) convert a C•G base pair into a T•A using the APOBEC1 cytidine deaminase. Fusion of APOBEC1 to *Streptococcus pyogenes* Cas9 (SpCas9) D10A mutant (nickase) and two copies of the uracil DNA glycosylase inhibitor (UGI), resulted in the creation of the SpBE4max enzyme (Koblan et al. 2018). A limitation of the current base editing technology is that the protospacer adjacent motif (PAM) must be appropriately positioned relative to the target base to ensure efficient editing (Rees and Liu 2018). Thus, there is a need to develop base editors with additional PAM compatibilities to increase the number of targetable bases in a genome. As such, SaCas9 has also been converted into a base editor to create SaBE4 (Rees and Liu 2018). In an analogous manner, we have created St1BE4max by exchanging SpCas9 D10A for St1Cas9 LMD9 D9A into the SpBE4max construct (Koblan et al. 2018). This created a potent CBE with novel targeting specificity due to the unique PAM of St1Cas9 (Fig. 3A).

Our data indicate that St1BE4max has an activity window similar to SaBE4, which is wider than SpBE4max, and sometimes extend upstream of the guide (Rees and Liu 2018) (Fig. 3A; Supplemental Data).

We then proceeded to test if St1Cas9 strain variants that display unique PAM preferences are also functional as CBEs. Indeed, LMG18311-, CNRZ1066-, and TH1477-based St1BE4max are efficient base editors at NNGCAA, NNACAA, and NNGAAA PAMs, respectively (Fig. 3B–D). St1BE4max variants were inactive at non-cognate PAMs indicating that they function in an orthogonal manner (Supplemental Fig. S5). We also generated an adenine base editor (St1ABEmax LMD9) to mediate the conversion of A•T to G•C in genomic DNA. We observed moderate editing efficiencies of St1ABEmax, a phenomenon also observed for SaABEmax, indicating that the ABEmax architecture is not fully compatible with these shorter Cas9s (Huang et al. 2019) (Fig. 3E). Nevertheless, these architectures can serve as a starting point for further improvements. Taken together, these data further demonstrate that St1Cas9 variants can be used as a scaffold to expand the targeting range of base editors.

In vivo genome editing using St1Cas9

The small size of St1Cas9 makes it potentially permissive for packaging holo-St1Cas9 (St1Cas9 + sgRNA) into adeno-associated virus (AAV) vectors for *in vivo* delivery. To test the cleavage activity of St1Cas9 *in vivo*, we used the hereditary tyrosinemia type I (HT-I) mouse model, a disease caused by a deficiency of fumarylacetoacetate hydrolase (FAH), the last enzyme of the tyrosine catabolic pathway (OMIM 276700) (Orphanet ORPHA:882) (Fig. 4A). *Fah*$^{-/-}$ mutant mice die as neonates with severe hepatic

dysfunction and kidney damage due to the accumulation of toxic metabolites unless treated with nitisone (NTBC), a drug that inhibits 4-hydroxyphenylpyruvate dioxygenase (HPD) upstream in the pathway (Fig. 4A) (Grompe 2017). Since genetic ablation of *Hpd* in mice can also prevent liver damage and lethality by creating a much milder HT-III phenotype (Endo et al. 1997; Pankowicz et al. 2016), we attempted to inactivate *Hpd* in our studies using St1Cas9.

To deliver holo-St1Cas9 to the liver, we generated a first set of AAV plasmids (AAV-St1Cas9 v1 and v2) containing a liver-specific promoter, sgRNA expression cassettes in opposite orientations and produced hepatotropic AAV serotype 8 (AAV8) vectors (Colella et al. 2018) (Supplemental Fig. S6A,B). We injected NTBC-treated *Fah*$^{-/-}$ mice at day 2 of life into the retro-orbital sinus with these vectors and isolated total liver DNA at day 28 post injection in treated mice (Fig. 4B; Supplemental Fig. S6A,B). The titration showed that the degree of target editing at two different exons of *Hpd* was substantial and dependent on the dose of AAV8-St1Cas9 (Supplemental Fig. S6A,B). We then evaluated if alternative AAV-St1Cas9 expression cassettes could further improve cleavage efficacy *in vivo* while minimizing vector size. In our best performing design (AAV-St1Cas9 v3), we engineered a liver-specific promoter (LP1b) by combining elements from the human apolipoprotein E/C-I gene locus control region (*ApoE*-HCR), a modified human α1 antitrypsin promoter (h*AAT*), an SV40 intron, and used a synthetic polyadenylation signal element (Fig. 4C) (Nathwani et al. 2006; McIntosh et al. 2013). These modifications increased cleavage efficacy markedly, especially at low AAV8 dose, and led to the creation of a vector of ~4.7 kb in size which is optimal for viral particle packaging (Fig.

297 4C,D) (Colella et al. 2018). It is worth noting that as the genomic DNA was extracted
298 from pieces of total livers, the effective activity is likely to be underestimated since
299 hepatocytes make up 70% of the liver's mass (Palaschak et al. 2019). Under the same
300 experimental conditions, the levels of *in vivo* editing achieved with AAV-St1Cas9 v3
301 were comparable to the ones obtained using the gold standard AAV-SaCas9 system
302 (Supplemental Fig. S6C) (Ran et al. 2015). Of note, since modifications made to AAV
303 plasmids can occasionally result in loss of potency of the recombinant AAV, we did not
304 alter the structure of the published SaCas9 vector (Ran et al. 2015) for this comparison.
305 Nevertheless, AAV8-mediated delivery into neonatal mice results in transient expression
306 (see discussion) which constitutes a stringent test of potency for the two nuclease
307 systems.
308
309 To test if AAV8-St1Cas9 v3 can achieve phenotypic correction *in vivo*, NTBC was
310 withdrawn shortly after weaning in the remaining subset of treated mice. Systemic
311 delivery via a single neonatal injection normalized the levels of excretion of
312 succinylacetone (SUAC), a toxic metabolite and a diagnostic marker for HT-I (Grompe
313 2017) (Fig. 4E). Even at the lower vector dose (5×10^{10}), we observed delayed but near
314 complete elimination of SUAC secretion 4 months following NTBC removal, which is
315 likely due to the potent selective growth advantage of targeted hepatocytes that can
316 extensively repopulate the diseased organ (Grompe 2017) (Fig. 4E). This is also reflected
317 by the increased levels of indels detected in liver samples over the same period (Fig. 4D).
318 Consequently, treatment rescued lethality in all mice while saline-treated animals had to
319 be killed after ~3 weeks as they met the weight loss criterion (Fig. 4F). Likewise,

glycemia and weight loss were normalized in the treatment groups (Fig. 4G,H). Therefore, AAV8-mediated delivery of St1Cas9 in neonatal mice can result in efficient DNA cleavage, stable genetic modification, and phenotypic correction by rewiring a metabolic pathway through gene inactivation.

To corroborate these findings we targeted *Pck1*, the gene encoding phosphoenolpyruvate carboxykinase 1, which plays a broad role in integrating hepatic energy metabolism and gluconeogenesis (Yang et al. 2009). Mice with a liver-specific deletion of the gene are viable but display an impaired response to fasting (She et al. 2000). Neonatal 2 days old C57BL/6N (wild-type) pups were injected with AAV8-St1Cas9 v3 targeting *Pck1* and at 6 weeks of age, they were fasted for 24 hours and killed for metabolic profiling and evaluating gene disruption efficacy (Supplemental Fig. S6D,E). Systemic delivery via a single neonatal injection resulted in substantial hepatic *Pck1* gene disruption (Supplemental Fig. S6D**)**. Plasma and hepatic triglyceride content were also markedly increased (Supplemental Fig. S6E). However, we found no change in circulating free fatty acid levels and hepatic glycogen stores were not depleted, suggesting that the observed phenotype may be intermediary to the one described in a prenatal hepatic knock-out model (Supplemental Fig. S6E) (She et al. 2000). We speculate that normal PCK1 in any non-targeted hepatocytes can partially compensate for the loss-of-function resulting from *in vivo* editing. Nevertheless, AAV8-mediated delivery of St1Cas9 in neonatal mice can efficiently disrupt the function of a key metabolic enzyme leading to clear and substantial phenotype *in vivo*. Collectively, these data support the notion that St1Cas9 can be engineered as a powerful tool for *in vivo* genome editing.

DISCUSSION

Here we report that St1Cas9 can be harnessed for robust and efficient genome editing *in vitro* and *in vivo*, thereby expanding the CRISPR-Cas toolbox. We optimized this system to create potent nucleases, transcription activators, and base editors. We further validated its use in mice by demonstrating efficient rewiring, rescue, and creation of metabolic defects using all-in-one AAV vectors. Our work offers a comprehensive analysis and highlights novel fields of application for this CRISPR-Cas9 platform in mammalian cells (Kleinstiver et al. 2015b; Muller et al. 2016). St1Cas9 also functions efficiently for labeling of chromosomal loci in human cells and in mouse zygotes to create animal models (Ma et al. 2015; Fujii et al. 2016). In other systems, such as mycobacteria and the plant *Arabidopsis thaliana*, St1Cas9 is at least comparable to, and can even outperform, SpCas9 (Steinert et al. 2015; Rock et al. 2017).

Structure-guided and random mutagenesis have been combined to successfully reprogram the PI domain of Cas9s to alter its specificity towards a distinct sequence, but also to relax its specificity (for example NNGRRT would become NNNRRT or NGG would become NGN) (Kleinstiver et al. 2015a; Kleinstiver et al. 2015b; Hu et al. 2018; Nishimasu et al. 2018). As expected, relaxed PAM recognition typically decreases genome-wide specificity by increasing the number of off-targets (Kleinstiver et al. 2015a; Nishimasu et al. 2018; Kleinstiver et al. 2019). As a corollary, off-target sites are generally low in number for Cas9s with longer PAMs versus with shorter ones (Kleinstiver et al. 2015b; Tsai et al. 2015; Kleinstiver et al. 2019). This highlights an

366 emerging connection between the length and complexity of the PAM versus the absolute
367 specificity of a Cas protein that warrants further exploration (Muller et al. 2016). In this
368 work, we engineered St1Cas9 variants with distinct PAM requirements and observed
369 limited cross-reactivity towards non-cognate PAMs. While the complete characterization
370 of PAM preference for each of these variants remains to be done, these data suggests a
371 stringent PAM requirement for St1Cas9s. Some level of flexibility in PAM recognition
372 has been observed and is to be expected for CRISPR-Cas systems in human cells. For
373 example, wild-type SpCas9 (consensus NGG) can also recognize NAG, NGA, NGT,
374 NGC with some, but not all, sgRNAs (Tsai et al. 2015; Nishimasu et al. 2018). Wild-type
375 SaCas9 (consensus NNGRRT) can cleave at non-canonical NNARRT PAMs (Kleinstiver
376 et al. 2015a). Finally, wild-type AsCas12a (consensus TTTV) can recognize non-
377 canonical GTTV and GCTV PAMs (Jacobsen et al. 2019). While this flexibility in PAM
378 recognition is a concern regarding potential off-target activity (Tsai et al. 2015), DNA
379 cleavage activity is typically much lower at these sites. Nevertheless, a comprehensive
380 genome-wide profiling of off-target cleavage remains to be performed for St1Cas9
381 variants. The recently described structure of St1Cas9 should facilitate the creation of
382 high-fidelity St1Cas9s (Slaymaker et al. 2016; Chen et al. 2017b; Vakulskas et al. 2018;
383 Fuchsbauer et al. 2019).
384
385 The engineering of CRISPR-Cas systems with unique PAM sequences is of utmost
386 importance and should not be guided uniquely by the absolute targeting range (the total
387 number of PAMs present in a genome) as the exact location of binding is most often key
388 for genome editing. Applications such as, disruption of small genetic elements, allele-

specific targeting, seamless gene correction via recombination, base editing, or gene correction via microhomology-mediated end joining require highly precise targeting (Canver et al. 2015; Rees and Liu 2018; Gyorgy et al. 2019; Iyer et al. 2019). To achieve single nucleotide precision in targeting, a plethora of Cas9 orthologs harboring both wild-type and altered PAM specificities will be needed. To illustrate the utility of St1Cas9 variants in such contexts, we identified several disease-causing mutations that could potentially be targeted in an allele-specific manner (Supplemental Fig. S7A). We also identified highly active St1Cas9 nucleases targeting narrow regions within the 5'UTR and first intron of the mouse albumin gene (Supplemental Fig. S7B,C). These sites are of particular interest since the albumin gene has been described as a safe-harbor locus for targeted integration of therapeutic transgenes and liver-directed protein replacement therapies (Sharma et al. 2015). Base editors using St1Cas9 variants could also be relevant to correct metabolic diseases (Supplemental Fig. S8).

Recombinant AAV vectors are prime *in vivo* gene delivery vectors for non-proliferative tissues. However, a limitation in the therapeutic use of AAV is the loss of episomal vector genomes from actively dividing cells resulting in transient expression of therapeutic transgenes. Hence, the combination of genome editing technology with AAV-mediated delivery could lead to permanent genome modification and positive therapeutic outcome in young patients when tissues, such as the liver and retina, are still growing (Li et al. 2011; Yang et al. 2016). As a side benefit, the elimination of vector genomes would lead to transient nuclease expression in proliferating tissues that likely prevents accumulation of mutations at off-target sites (Li et al. 2011; Yang et al. 2016). In this

perspective, the development of alternative *in vivo* genome editing platforms based on orthologous CRISPR-Cas systems would further increase the options available for therapeutic interventions.

METHODS

Cell culture and transfection

K562 were obtained from the ATCC (CCL-243) and maintained at 37 °C under 5% CO_2 in RPMI medium supplemented with 10% FBS, penicillin-streptomycin and GlutaMAX. Neuro-2a were obtained from the ATCC and maintained at 37 °C under 5% CO_2 in DMEM medium supplemented with 10% FBS, penicillin-streptomycin and GlutaMAX. All cell lines are tested for absence of mycoplasma contamination. Cells (2 x 10^5 per transfection) were transfected using the Amaxa 4D-Nucleofector (Lonza) per manufacturer's recommendations. Unless otherwise specified, 0.5μg and 1μg of single vector constructs driving the expression of both the sgRNA and St1Cas9 variants (nucleases or base editors) were used for transient transfections in Neuro-2a and K562 cells, respectively. K562 cell lines expressing St1Cas9 from the *AAVS1* safe harbor locus were generated as described (Dalvai et al. 2015; Agudelo et al. 2017). Briefly, simultaneous selection and cloning was performed for 10 days in methylcellulose-based semi-solid RPMI medium supplemented with 0.5 μg/ml puromycin starting 3 days post-transfection. Clones were picked and expanded in 96 wells for 3 days and transferred to 12-well plates for another 3 days before cells were harvested for western blot analysis.

435

436 **St1Cas9 strain variants**

437 Sequences of St1Cas9 variants were retrieved from NCBI's Identical Protein Groups
438 (IPG) resource which contained 29 unique protein sequences at the time of analysis.
439 Predicted PAM sequences for St1Cas9 LMD9, LMG18311, CNRZ1066 were previously
440 published (Bolotin et al. 2005; Deveau et al. 2008; Chen et al. 2014). Predictions for
441 St1Cas9s related to TH1477 and MTH17CL396 originated from
442 https://github.com/mitmedialab/SPAMALOT (Chatterjee et al. 2018). Alignments were
443 performed using Clustal Omega (Sievers et al. 2011) in combination with the sequence
444 alignment renderer ESPript 3 (Robert and Gouet 2014).

445

446 **Structural analysis of PAM specificity**

447 Coot and PISA were used to analyze the 3D structures (Krissinel and Henrick 2007).
448 UCSF ChimeraX was used to prepare the figures (Goddard et al. 2018).

449

450 **Genome editing vectors**

451 Vectors for *in vitro* and *in vivo* genome editing with the CRISPR1-Cas9 (St1Cas9)
452 system of *S. thermophilus* generated in this study are available from Addgene
453 (Supplemental Fig. S9). Protein and DNA sequences for all St1Cas9 ORFs are available
454 in Supplemental Tables S1-5. The mammalian expression vector for St1Cas9 (LMD9)
455 fused to SV40 NLS sequences at the N- and C-terminus (MSP1594_2x_NLS; Addgene
456 plasmid #110625) was constructed from MSP1594 (Kleinstiver et al. 2015b) (Addgene
457 plasmid #65775, a gift from Keith Joung). The U6-driven sgRNA expression cassettes for

St1Cas9 (LMD9) (v1, v2, v3) (St1Cas9_LMD-9_sgRNA_pUC19; Addgene plasmid #110627) were synthesized as gBlock gene fragments (Integrated DNA Technologies) and cloned into pUC19 (Supplemental Table S11). BPK2301 (Kleinstiver et al. 2015b) (v0) (Addgene plasmid #65778, a gift from Keith Joung) was used to compare St1Cas9 sgRNA architectures. The single vector mammalian expression system containing a CAG promoter-driven St1Cas9 LMD9 and its U6-driven sgRNA (U6_sgRNA_CAG_hSt1Cas9_LMD9; Addgene plasmid #110626) was built from the above-described plasmids. LMG18311, CNRZ1066, TH1477, MTH17CL396 C-terminal sequences were synthesized as gBlock gene fragments (Integrated DNA Technologies) and subcloned into U6_sgRNA_CAG_hSt1Cas9_LMD9 to produce the chimeric vectors (Addgene plasmids #136653, #136651, #136655, #136656).

Base editors were constructed into U6_sgRNA_CAG_hSt1Cas9_LMD9 (or the chimeric variants) using fragments derived from pCMV_BE4max_3xHA and pCMV_ABEmax_3xHA (Koblan et al. 2018) (Addgene plasmids #112096 and #112098, a gift from David Liu). Protein and DNA sequences for all St1Cas9 base editors are available in Supplemental Tables S6-10. St1Cas9BE4max (Addgene plasmids #136652, #136654, #136657, #136659) and ABEmax (Addgene plasmid #136660) variants are available for distribution.

The single vector rAAV-St1Cas9 LMD9 systems containing liver-specific promoters were assembled from the above-described components into a derivative of pX602 (Ran et al. 2015) (Addgene plasmid #61593, a gift from Feng Zhang) containing a deletion within

481 the backbone to eliminate BsmBI restriction sites. The LP1b promoter was engineered by
482 combining elements from previously described AAV expression cassettes (Nathwani et
483 al. 2006; McIntosh et al. 2013) (Supplemental Table S12). We deposited the most active
484 version of this vector (v3) (pAAV_LP1B_St1Cas9_LMD-9_SpA_U6_sgRNA; Addgene
485 plasmid #110624).
486
487 To establish clonal K562 cell lines constitutively expressing C-terminally tagged St1Cas9
488 under the control of an h*PGK1* promoter, the Cas9 ORF from MSP1594_2x_NLS was
489 subcloned into AAVS1_Puro_PGK1_3xFLAG_Twin_Strep (Dalvai et al. 2015)
490 (Addgene plasmid #68375).
491
492 The CRISPOR (Haeussler et al. 2016) web tool was used to design guide sequences
493 against mouse and human targets St1Cas9 LMD9. For St1Cas9 variants the guides were
494 identified by manual inspection of target sequences. Guide sequences are available in
495 Supplemental Tables S13-18.
496
497 **Surveyor nuclease, TIDE, and base editing assays**
498 Genomic DNA from 2.5 x 10^5 cells was extracted with 250 µl of QuickExtract DNA
499 extraction solution (Lucigen) per manufacturer's recommendations. The various loci were
500 amplified by 30 cycles of PCR using the primers described in Supplemental Table S19.
501 Assays were performed with the Surveyor mutation detection kit (Transgenomics) as
502 described (Guschin et al. 2010; Agudelo et al. 2017). Samples were separated on 10%
503 PAGE gels in TBE buffer. Gels were imaged using a ChemiDoc MP (Bio-Rad) system

and quantifications were performed using the Image lab software (Bio-Rad). TIDE analysis was performed using a significance cut-off value for decomposition of $p<0.001$ (Brinkman et al. 2014). EditR (Kluesner et al. 2018) was used to quantify base editing from Sanger sequencing reads with the p value cutoff set to 0.01. Under these settings, any editing levels equal or lower than 5% is considered background. All chromatograms are available as Supplemental Data.

Recombinant adeno-associated virus production

Production of recombinant adeno-associated viral vectors was performed by the triple plasmid transfection method essentially as described (Gray et al. 2011). Briefly, HEK293T17 cells were transfected using polyethylenimine (PEI, Polysciences) with helper plasmid pxx-680 (A gift from R.J. Samulski), the rep/cap hybrid plasmid pAAV2/8 (A gift from James Wilson) and the rAAV vector plasmid. Twenty-four hours post-transfection, media was replaced with growth media without FBS, and cells were harvested 24 hours later. rAAV particles were extracted from cell extracts by freeze/thaw cycles and purified on a discontinuous iodixanol gradient. Virus were resuspended in PBS 320 mM NaCl + 5% D-sorbitol + 0.001% pluronic acid (F-68), aliquoted and stored at $^{-}80^{o}$C. rAAV were titrated by qPCR (Roche) using SYBR Green and ITR primers as described (Aurnhammer et al. 2012). The yields for all vectors varied between 1×10^{13} and 2×10^{13} vg/ml. The purity of the viral preparations was determined by SDS-PAGE analysis on a 10% stain free gel (Bio-Rad) in Tris-Glycine-SDS buffer (Supplemental Fig. S10). ITR integrity was assessed following a BssHII digestion of the AAV plasmid.

The vector core facility at the Canadian neurophotonics platform (molecular tools) produced the rAAV8s.

Animal experiments (*Fah*$^{-/-}$ mouse model)

Fah$^{-/-}$ mice (Grompe et al. 1993) on a C57BL/6 genetic background were group-housed and fed a standard chow diet (Harlan #2018SX) with free access to food and water. *Fah*$^{-/-}$ mice drinking water was supplemented with 7.5 mg (2-(2-nitro-4-trifluoromethylbenzoyl)-1,3-cyclohexanedione) (NTBC)/L and pH was adjusted to 7.0. Mice were exposed to a 12:12-h dark-light cycle and kept under an ambient temperature of 23 ± 1 °C. Animals were cared for and handled according to the *Canadian Guide for the Care and Use of Laboratory Animals.* The Université Laval Animal Care and Use Committee approved the procedures.

Two days old neonatal mice were injected intravenously in the retro-orbital sinus (Yardeni et al. 2011) with different doses of rAAV8 or saline in a total volume of 20 µL. Mice were weaned at 21 days of age and NTBC was removed 7 days later. Body weight and glycemia were monitored daily following NTBC removal. Mice were not fasted for measurement of glycemia, data collection occurred between 9-10 am. Animals were killed by cardiac puncture under anesthesia at predetermined time points or when weight loss reached 20% of body weight. Livers were snap frozen for downstream applications.

Urine collection and succinylacetone quantification

548 Urine from groups of 3-4 mice was collected overnight in metabolic cages (Tecniplast)
549 15 days and 4 months after NTBC removal. Urine was centrifuged at 2000 rpm for 5
550 minutes, aliquoted and frozen at -80°C. Succinylacetone was quantified in urine samples
551 by a sensitive method using gas chromatography–mass spectrometry (GC-MS) as
552 previously described (Cyr et al. 2006). The biochemical genetics laboratory at the centre
553 hospitalier universitaire de Sherbrooke performed the analyses.
554

555 Methods related to transcription activation (Supplemental Fig. S2) and experiments
556 performed in *C57BL/6N* mice (Supplemental Fig. S6) are described in the Supplemental
557 Methods section.

558

559 ## DATA ACCESS

560 All vectors generated in this study have been deposited to Addgene. All raw Sanger
561 sequencing data generated in this study are available as Supplemental Data.
562

563 ## ACKNOWLEDGMENTS

564 This study was supported by grants from the Canadian Institutes of Health Research
565 (CIHR) to M.L. and Y.D. and by the Banting Research Foundation to Y.D. S.M.
566 acknowledges funding from NSERC. S.M. holds a Tier 1 Canada Research Chair in
567 Bacteriophages. A.G. acknowledges funding from the French National Research Agency
568 (ANR-18-CE11-0016-01). UCSF ChimeraX that was used for molecular graphics and
569 analyses is developed by the Resource for Biocomputing, Visualization, and Informatics

at the University of California, San Francisco, and receive support from NIH R01-GM129325 and P41-GM103311. Salary support was provided by the Fonds de la recherche du Québec-Santé (FRQS) to M.L. and Y.D. D.A. holds a Vanier Canada graduate scholarship. S.L. holds a Frederick Banting and Charles Best Canada graduate scholarship. A.D. and J-F.R. hold graduate training awards from the Fonds de la recherche du Québec-Santé (FRQS). J-F.R is also supported by the Fondation du Grand défi Pierre Lavoie. We thank Marie-Ève Paquet and the skilled vector core facility staff at the Canadian neurophotonics platform for AAV8 production. Robert Tanguay provided the mouse model of HT-I, nitisone, expertise and support.

AUTHOR CONTRIBUTIONS

Conceptualization, D.A., S.C., M.V., A.D., J-F. R., S.M., A.G., and Y.D.; Methodology, D.A., S.C., M.V., A.D., J-F. R., S.L., J.L., M.M., D.C., P.J.W., M.L., A.G., and Y.D.; Investigation, D.A., S.C., M.V., A.D., J-F. R., S.L., A.D., J.L., M.M., D.C.; Writing – Original Draft, Y.D.; Writing – Review and Editing, all authors; Supervision, P.J.W., M.L., Y.D.; Funding Acquisition, M.L., S.M., A.G., and Y.D. All authors read and approved the final manuscript.

DISCLOSURE DECLARATION

An international patent application has been filed in relation to this work. Y.D. is named as an inventor.

REFERENCES

Agudelo D, Duringer A, Bozoyan L, Huard CC, Carter S, Loehr J, Synodinou D, Drouin M, Salsman J, Dellaire G et al. 2017. Marker-free coselection for CRISPR-driven genome editing in human cells. *Nat Methods* **14**: 615-620.

Aurnhammer C, Haase M, Muether N, Hausl M, Rauschhuber C, Huber I, Nitschko H, Busch U, Sing A, Ehrhardt A et al. 2012. Universal real-time PCR for the detection and quantification of adeno-associated virus serotype 2-derived inverted terminal repeat sequences. *Hum Gene Ther Methods* **23**: 18-28.

Barrangou R, Horvath P. 2017. A decade of discovery: CRISPR functions and applications. *Nat Microbiol* **2**: 17092.

Bolotin A, Quinquis B, Sorokin A, Ehrlich SD. 2005. Clustered regularly interspaced short palindrome repeats (CRISPRs) have spacers of extrachromosomal origin. *Microbiology* **151**: 2551-2561.

614 Briner AE, Donohoue PD, Gomaa AA, Selle K, Slorach EM, Nye CH, Haurwitz RE,
615 Beisel CL, May AP, Barrangou R. 2014. Guide RNA functional modules direct Cas9
616 activity and orthogonality. *Mol Cell* **56**: 333-339.

617 Brinkman EK, Chen T, Amendola M, van Steensel B. 2014. Easy quantitative assessment
618 of genome editing by sequence trace decomposition. *Nucleic Acids Res* **42**: e168.

619 Canver MC, Smith EC, Sher F, Pinello L, Sanjana NE, Shalem O, Chen DD, Schupp PG,
620 Vinjamur DS, Garcia SP et al. 2015. BCL11A enhancer dissection by Cas9-mediated in
621 situ saturating mutagenesis. *Nature* **527**: 192-197.

622 Chari R, Mali P, Moosburner M, Church GM. 2015. Unraveling CRISPR-Cas9 genome
623 engineering parameters via a library-on-library approach. *Nat Methods* **12**: 823-826.

624 Chatterjee P, Jakimo N, Jacobson JM. 2018. Minimal PAM specificity of a highly similar
625 SpCas9 ortholog. *Sci Adv* **4**: eaau0766.

626 Chavez A, Scheiman J, Vora S, Pruitt BW, Tuttle M, E PRI, Lin S, Kiani S, Guzman CD,
627 Wiegand DJ et al. 2015. Highly efficient Cas9-mediated transcriptional programming.
628 *Nat Methods* **12**: 326-328.

629 Chen F, Ding X, Feng Y, Seebeck T, Jiang Y, Davis GD. 2017a. Targeted activation of
630 diverse CRISPR-Cas systems for mammalian genome editing via proximal CRISPR
631 targeting. *Nat Commun* **8**: 14958.

632 Chen H, Choi J, Bailey S. 2014. Cut site selection by the two nuclease domains of the
633 Cas9 RNA-guided endonuclease. *J Biol Chem* **289**: 13284-13294.

634 Chen JS, Dagdas YS, Kleinstiver BP, Welch MM, Sousa AA, Harrington LB, Sternberg
635 SH, Joung JK, Yildiz A, Doudna JA. 2017b. Enhanced proofreading governs CRISPR-
636 Cas9 targeting accuracy. *Nature* doi:10.1038/nature24268.

637 Colella P, Ronzitti G, Mingozzi F. 2018. Emerging Issues in AAV-Mediated In Vivo
638 Gene Therapy. *Mol Ther Methods Clin Dev* **8**: 87-104.

639 Cong L, Ran FA, Cox D, Lin S, Barretto R, Habib N, Hsu PD, Wu X, Jiang W,
640 Marraffini LA et al. 2013. Multiplex genome engineering using CRISPR/Cas systems.
641 *Science* **339**: 819-823.

642 Cyr D, Giguere R, Villain G, Lemieux B, Drouin R. 2006. A GC/MS validated method
643 for the nanomolar range determination of succinylacetone in amniotic fluid and plasma:
644 an analytical tool for tyrosinemia type I. *J Chromatogr B Analyt Technol Biomed Life Sci*
645 **832**: 24-29.

646 Dalvai M, Loehr J, Jacquet K, Huard CC, Roques C, Herst P, Cote J, Doyon Y. 2015. A
647 Scalable Genome-Editing-Based Approach for Mapping Multiprotein Complexes in
648 Human Cells. *Cell Rep* **13**: 621-633.

649 Deveau H, Barrangou R, Garneau JE, Labonte J, Fremaux C, Boyaval P, Romero DA,
650 Horvath P, Moineau S. 2008. Phage response to CRISPR-encoded resistance in
651 Streptococcus thermophilus. *J Bacteriol* **190**: 1390-1400.

652 Edraki A, Mir A, Ibraheim R, Gainetdinov I, Yoon Y, Song CQ, Cao Y, Gallant J, Xue
653 W, Rivera-Perez JA et al. 2019. A Compact, High-Accuracy Cas9 with a Dinucleotide
654 PAM for In Vivo Genome Editing. *Mol Cell* **73**: 714-726 e714.

655 Endo F, Kubo S, Awata H, Kiwaki K, Katoh H, Kanegae Y, Saito I, Miyazaki J,
656 Yamamoto T, Jakobs C et al. 1997. Complete rescue of lethal albino c14CoS mice by
657 null mutation of 4-hydroxyphenylpyruvate dioxygenase and induction of apoptosis of
658 hepatocytes in these mice by in vivo retrieval of the tyrosine catabolic pathway. *J Biol*
659 *Chem* **272**: 24426-24432.

660 Esvelt KM, Mali P, Braff JL, Moosburner M, Yaung SJ, Church GM. 2013. Orthogonal
661 Cas9 proteins for RNA-guided gene regulation and editing. *Nat Methods* **10**: 1116-1121.

662 Fuchsbauer O, Swuec P, Zimberger C, Amigues B, Levesque S, Agudelo D, Duringer A,
663 Chaves-Sanjuan A, Spinelli S, Rousseau GM et al. 2019. Cas9 Allosteric Inhibition by
664 the Anti-CRISPR Protein AcrIIA6. *Mol Cell* doi:10.1016/j.molcel.2019.09.012.

665 Fujii W, Kakuta S, Yoshioka S, Kyuwa S, Sugiura K, Naito K. 2016. Zygote-mediated
666 generation of genome-modified mice using Streptococcus thermophilus 1-derived
667 CRISPR/Cas system. *Biochem Biophys Res Commun* **477**: 473-476.

668 Garcia B, Lee J, Edraki A, Hidalgo-Reyes Y, Erwood S, Mir A, Trost CN, Seroussi U,
669 Stanley SY, Cohn RD et al. 2019. Anti-CRISPR AcrIIA5 Potently Inhibits All Cas9
670 Homologs Used for Genome Editing. *Cell Rep* **29**: 1739-1746 e1735.

671 Goddard TD, Huang CC, Meng EC, Pettersen EF, Couch GS, Morris JH, Ferrin TE.
672 2018. UCSF ChimeraX: Meeting modern challenges in visualization and analysis.
673 *Protein Sci* **27**: 14-25.

674 Gray SJ, Choi VW, Asokan A, Haberman RA, McCown TJ, Samulski RJ. 2011.
675 Production of recombinant adeno-associated viral vectors and use in in vitro and in vivo
676 administration. *Curr Protoc Neurosci* **Chapter 4**: Unit 4 17.

677 Grompe M. 2017. Fah Knockout Animals as Models for Therapeutic Liver Repopulation.
678 *Adv Exp Med Biol* **959**: 215-230.

679 Grompe M, al-Dhalimy M, Finegold M, Ou CN, Burlingame T, Kennaway NG, Soriano
680 P. 1993. Loss of fumarylacetoacetate hydrolase is responsible for the neonatal hepatic
681 dysfunction phenotype of lethal albino mice. *Genes Dev* **7**: 2298-2307.

682 Guschin DY, Waite AJ, Katibah GE, Miller JC, Holmes MC, Rebar EJ. 2010. A rapid
683 and general assay for monitoring endogenous gene modification. *Methods Mol Biol* **649**:
684 247-256.

685 Gyorgy B, Nist-Lund C, Pan B, Asai Y, Karavitaki KD, Kleinstiver BP, Garcia SP,
686 Zaborowski MP, Solanes P, Spataro S et al. 2019. Allele-specific gene editing prevents
687 deafness in a model of dominant progressive hearing loss. *Nat Med* doi:10.1038/s41591-
688 019-0500-9.

689 Haeussler M, Schonig K, Eckert H, Eschstruth A, Mianne J, Renaud JB, Schneider-
690 Maunoury S, Shkumatava A, Teboul L, Kent J et al. 2016. Evaluation of off-target and
691 on-target scoring algorithms and integration into the guide RNA selection tool CRISPOR.
692 *Genome Biol* **17**: 148.

693 Hille F, Richter H, Wong SP, Bratovic M, Ressel S, Charpentier E. 2018. The Biology of
694 CRISPR-Cas: Backward and Forward. *Cell* **172**: 1239-1259.

695 Hu JH, Miller SM, Geurts MH, Tang W, Chen L, Sun N, Zeina CM, Gao X, Rees HA,
696 Lin Z et al. 2018. Evolved Cas9 variants with broad PAM compatibility and high DNA
697 specificity. *Nature* **556**: 57-63.

698 Huang TP, Zhao KT, Miller SM, Gaudelli NM, Oakes BL, Fellmann C, Savage DF, Liu
699 DR. 2019. Circularly permuted and PAM-modified Cas9 variants broaden the targeting
700 scope of base editors. *Nat Biotechnol* **37**: 626-631.

701 Hynes AP, Rousseau GM, Agudelo D, Goulet A, Amigues B, Loehr J, Romero DA,
702 Fremaux C, Horvath P, Doyon Y et al. 2018. Widespread anti-CRISPR proteins in
703 virulent bacteriophages inhibit a range of Cas9 proteins. *Nat Commun* **9**: 2919.

704 Ibraheim R, Song CQ, Mir A, Amrani N, Xue W, Sontheimer EJ. 2018. All-in-one
705 adeno-associated virus delivery and genome editing by Neisseria meningitidis Cas9 in
706 vivo. *Genome Biol* **19**: 137.

707 Iyer S, Suresh S, Guo D, Daman K, Chen JCJ, Liu P, Zieger M, Luk K, Roscoe BP,
708 Mueller C et al. 2019. Precise therapeutic gene correction by a simple nuclease-induced
709 double-stranded break. *Nature* **568**: 561-565.

710 Jacobsen T, Liao C, Beisel CL. 2019. The Acidaminococcus sp. Cas12a nuclease
711 recognizes GTTV and GCTV as non-canonical PAMs. *FEMS Microbiol Lett* **366**.

712 Jinek M, Chylinski K, Fonfara I, Hauer M, Doudna JA, Charpentier E. 2012. A
713 programmable dual-RNA-guided DNA endonuclease in adaptive bacterial immunity.
714 *Science* **337**: 816-821.

715 Kim E, Koo T, Park SW, Kim D, Kim K, Cho HY, Song DW, Lee KJ, Jung MH, Kim S
716 et al. 2017. In vivo genome editing with a small Cas9 orthologue derived from
717 Campylobacter jejuni. *Nat Commun* **8**: 14500.

718 Kleinstiver BP, Prew MS, Tsai SQ, Nguyen NT, Topkar VV, Zheng Z, Joung JK. 2015a.
719 Broadening the targeting range of Staphylococcus aureus CRISPR-Cas9 by modifying
720 PAM recognition. *Nat Biotechnol* **33**: 1293-1298.

721 Kleinstiver BP, Prew MS, Tsai SQ, Topkar VV, Nguyen NT, Zheng Z, Gonzales AP, Li
722 Z, Peterson RT, Yeh JR et al. 2015b. Engineered CRISPR-Cas9 nucleases with altered
723 PAM specificities. *Nature* **523**: 481-485.

724 Kleinstiver BP, Sousa AA, Walton RT, Tak YE, Hsu JY, Clement K, Welch MM, Horng
725 JE, Malagon-Lopez J, Scarfo I et al. 2019. Engineered CRISPR-Cas12a variants with
726 increased activities and improved targeting ranges for gene, epigenetic and base editing.
727 *Nat Biotechnol* doi:10.1038/s41587-018-0011-0.

728 Kluesner MG, Nedveck DA, Lahr WS, Garbe JR, Abrahante JE, Webber BR, Moriarity
729 BS. 2018. EditR: A Method to Quantify Base Editing from Sanger Sequencing. *CRISPR*
730 *J* **1**: 239-250.

731 Koblan LW, Doman JL, Wilson C, Levy JM, Tay T, Newby GA, Maianti JP, Raguram A,
732 Liu DR. 2018. Improving cytidine and adenine base editors by expression optimization
733 and ancestral reconstruction. *Nat Biotechnol* **36**: 843-846.

734 Komor AC, Badran AH, Liu DR. 2017. CRISPR-Based Technologies for the
735 Manipulation of Eukaryotic Genomes. *Cell* **169**: 559.

736 Koonin EV, Makarova KS, Zhang F. 2017. Diversity, classification and evolution of
737 CRISPR-Cas systems. *Curr Opin Microbiol* **37**: 67-78.

738 Krissinel E, Henrick K. 2007. Inference of macromolecular assemblies from crystalline
739 state. *J Mol Biol* **372**: 774-797.

740 Lau CH, Suh Y. 2017. In vivo genome editing in animals using AAV-CRISPR system:
741 applications to translational research of human disease. *F1000Res* **6**: 2153.

742 Leenay RT, Maksimchuk KR, Slotkowski RA, Agrawal RN, Gomaa AA, Briner AE,
743 Barrangou R, Beisel CL. 2016. Identifying and Visualizing Functional PAM Diversity
744 across CRISPR-Cas Systems. *Mol Cell* **62**: 137-147.

745 Li H, Haurigot V, Doyon Y, Li T, Wong SY, Bhagwat AS, Malani N, Anguela XM,
746 Sharma R, Ivanciu L et al. 2011. In vivo genome editing restores haemostasis in a mouse
747 model of haemophilia. *Nature* **475**: 217-221.

748 Ma H, Naseri A, Reyes-Gutierrez P, Wolfe SA, Zhang S, Pederson T. 2015. Multicolor
749 CRISPR labeling of chromosomal loci in human cells. *Proc Natl Acad Sci U S A* **112**:
750 3002-3007.

751 Maeder ML, Stefanidakis M, Wilson CJ, Baral R, Barrera LA, Bounoutas GS, Bumcrot
752 D, Chao H, Ciulla DM, DaSilva JA et al. 2019. Development of a gene-editing approach
753 to restore vision loss in Leber congenital amaurosis type 10. *Nat Med* **25**: 229-233.

754 Makarova KS, Wolf YI, Koonin EV. 2018. Classification and Nomenclature of CRISPR-
755 Cas Systems: Where from Here? *CRISPR J* **1**: 325-336.

McIntosh J, Lenting PJ, Rosales C, Lee D, Rabbanian S, Raj D, Patel N, Tuddenham EG, Christophe OD, McVey JH et al. 2013. Therapeutic levels of FVIII following a single peripheral vein administration of rAAV vector encoding a novel human factor VIII variant. *Blood* **121**: 3335-3344.

Mir A, Edraki A, Lee J, Sontheimer EJ. 2018. Type II-C CRISPR-Cas9 Biology, Mechanism, and Application. *ACS Chem Biol* **13**: 357-365.

Muller M, Lee CM, Gasiunas G, Davis TH, Cradick TJ, Siksnys V, Bao G, Cathomen T, Mussolino C. 2016. Streptococcus thermophilus CRISPR-Cas9 Systems Enable Specific Editing of the Human Genome. *Mol Ther* **24**: 636-644.

Nathwani AC, Gray JT, Ng CY, Zhou J, Spence Y, Waddington SN, Tuddenham EG, Kemball-Cook G, McIntosh J, Boon-Spijker M et al. 2006. Self-complementary adeno-associated virus vectors containing a novel liver-specific human factor IX expression cassette enable highly efficient transduction of murine and nonhuman primate liver. *Blood* **107**: 2653-2661.

Nishimasu H, Cong L, Yan WX, Ran FA, Zetsche B, Li Y, Kurabayashi A, Ishitani R, Zhang F, Nureki O. 2015. Crystal Structure of Staphylococcus aureus Cas9. *Cell* **162**: 1113-1126.

Nishimasu H, Shi X, Ishiguro S, Gao L, Hirano S, Okazaki S, Noda T, Abudayyeh OO, Gootenberg JS, Mori H et al. 2018. Engineered CRISPR-Cas9 nuclease with expanded targeting space. *Science* **361**: 1259-1262.

776 Palaschak B, Herzog RW, Markusic DM. 2019. AAV-Mediated Gene Delivery to the
777 Liver: Overview of Current Technologies and Methods. *Methods Mol Biol* **1950**: 333-
778 360.

779 Pankowicz FP, Barzi M, Legras X, Hubert L, Mi T, Tomolonis JA, Ravishankar M, Sun
780 Q, Yang D, Borowiak M et al. 2016. Reprogramming metabolic pathways in vivo with
781 CRISPR/Cas9 genome editing to treat hereditary tyrosinaemia. *Nat Commun* **7**: 12642.

782 Ran FA, Cong L, Yan WX, Scott DA, Gootenberg JS, Kriz AJ, Zetsche B, Shalem O, Wu
783 X, Makarova KS et al. 2015. In vivo genome editing using Staphylococcus aureus Cas9.
784 *Nature* **520**: 186-191.

785 Rees HA, Liu DR. 2018. Base editing: precision chemistry on the genome and
786 transcriptome of living cells. *Nat Rev Genet* **19**: 770-788.

787 Robert X, Gouet P. 2014. Deciphering key features in protein structures with the new
788 ENDscript server. *Nucleic Acids Res* **42**: W320-324.

789 Rock JM, Hopkins FF, Chavez A, Diallo M, Chase MR, Gerrick ER, Pritchard JR,
790 Church GM, Rubin EJ, Sassetti CM et al. 2017. Programmable transcriptional repression
791 in mycobacteria using an orthogonal CRISPR interference platform. *Nat Microbiol* **2**:
792 16274.

793 Schneller JL, Lee CM, Bao G, Venditti CP. 2017. Genome editing for inborn errors of
794 metabolism: advancing towards the clinic. *BMC Med* **15**: 43.

795 Sharma R, Anguela XM, Doyon Y, Wechsler T, DeKelver RC, Sproul S, Paschon DE,
796 Miller JC, Davidson RJ, Shivak D et al. 2015. In vivo genome editing of the albumin
797 locus as a platform for protein replacement therapy. *Blood* **126**: 1777-1784.

798 She P, Shiota M, Shelton KD, Chalkley R, Postic C, Magnuson MA. 2000.
799 Phosphoenolpyruvate carboxykinase is necessary for the integration of hepatic energy
800 metabolism. *Mol Cell Biol* **20**: 6508-6517.

801 Shmakov S, Smargon A, Scott D, Cox D, Pyzocha N, Yan W, Abudayyeh OO,
802 Gootenberg JS, Makarova KS, Wolf YI et al. 2017. Diversity and evolution of class 2
803 CRISPR-Cas systems. *Nat Rev Microbiol* **15**: 169-182.

804 Sievers F, Wilm A, Dineen D, Gibson TJ, Karplus K, Li W, Lopez R, McWilliam H,
805 Remmert M, Soding J et al. 2011. Fast, scalable generation of high-quality protein
806 multiple sequence alignments using Clustal Omega. *Mol Syst Biol* **7**: 539.

807 Slaymaker IM, Gao L, Zetsche B, Scott DA, Yan WX, Zhang F. 2016. Rationally
808 engineered Cas9 nucleases with improved specificity. *Science* **351**: 84-88.

809 Steinert J, Schiml S, Fauser F, Puchta H. 2015. Highly efficient heritable plant genome
810 engineering using Cas9 orthologues from Streptococcus thermophilus and
811 Staphylococcus aureus. *Plant J* **84**: 1295-1305.

812 Tsai SQ, Zheng Z, Nguyen NT, Liebers M, Topkar VV, Thapar V, Wyvekens N, Khayter
813 C, Iafrate AJ, Le LP et al. 2015. GUIDE-seq enables genome-wide profiling of off-target
814 cleavage by CRISPR-Cas nucleases. *Nat Biotechnol* **33**: 187-197.

Tycko J, Barrera LA, Huston NC, Friedland AE, Wu X, Gootenberg JS, Abudayyeh OO, Myer VE, Wilson CJ, Hsu PD. 2018. Pairwise library screen systematically interrogates Staphylococcus aureus Cas9 specificity in human cells. *Nat Commun* **9**: 2962.

Vakulskas CA, Dever DP, Rettig GR, Turk R, Jacobi AM, Collingwood MA, Bode NM, McNeill MS, Yan S, Camarena J et al. 2018. A high-fidelity Cas9 mutant delivered as a ribonucleoprotein complex enables efficient gene editing in human hematopoietic stem and progenitor cells. *Nat Med* **24**: 1216-1224.

Yang J, Kalhan SC, Hanson RW. 2009. What is the metabolic role of phosphoenolpyruvate carboxykinase? *J Biol Chem* **284**: 27025-27029.

Yang Y, Wang L, Bell P, McMenamin D, He Z, White J, Yu H, Xu C, Morizono H, Musunuru K et al. 2016. A dual AAV system enables the Cas9-mediated correction of a metabolic liver disease in newborn mice. *Nat Biotechnol* **34**: 334-338.

Yardeni T, Eckhaus M, Morris HD, Huizing M, Hoogstraten-Miller S. 2011. Retro-orbital injections in mice. *Lab Anim (NY)* **40**: 155-160.

Zetsche B, Gootenberg JS, Abudayyeh OO, Slaymaker IM, Makarova KS, Essletzbichler P, Volz SE, Joung J, van der Oost J, Regev A et al. 2015. Cpf1 is a single RNA-guided endonuclease of a class 2 CRISPR-Cas system. *Cell* **163**: 759-771.

Figure 1. Functional PAM sequences for robust and potent DNA cleavage by St1Cas9 LMD9 in mammalian cells. (A) Schematic representations of St1Cas9 LMD9 flanked by nuclear localization signals (NLS) and its engineered sgRNA (v1). Nucleotide sequence and functional modules are depicted; crRNA (green), loop (grey), tracrRNA (blue), mutated nucleotides (orange). (B) K562 cells stably expressing St1Cas9 were transfected with indicated sgRNA expression vectors at increasing doses and TIDE assays were performed 3 days later to determine the frequency of indels. An expression vector encoding EGFP (-) was used as a negative control. The experiment was performed twice and yielded equivalent results, only one is shown. (C) Screening for guides targeting St1Cas9 LMD9 to various PAMs was done by transient transfections in K562 (solid shapes) and Neuro-2a (open shapes) cells using single vector constructs driving the expression of St1Cas9 and its sgRNA. Surveyor assays were performed 3 days later to determine the frequency of indels. An expression vector encoding EGFP (-) was used as a negative control. (See also Supplemental Fig. S1).

Figure 2. Structural basis for PAM specificity of engineered St1Cas9 variants with expanded targeting range. (A) Schematic representation of St1Cas9 hybrid proteins containing the N-terminal of LMD9 and the C-terminal domains (WED + PI) of LMG18311 or CNRZ1066. To determine the activity of St1Cas9 variants programmed with sgRNAs compatible with different PAMs, K562 cells were transiently transfected with single vector constructs driving expression of St1Cas9 and its sgRNA. For each PAM and nuclease combination, four different sgRNAs (targets) were tested. Surveyor assays were performed 3 days later to determine the frequency of indels. An expression vector encoding EGFP (-) was used as a negative control. The experiment was performed twice and yielded equivalent results, only one is shown. (B) Close-up view of the 5'-GCAGAAA-3' PAM bound to the St1Cas9 (DGCC7010) PI domain (PDB: 6RJD). The target (turquoise) and non-target (blue) strands are shown as sticks (the phosphate-sugar backbones are also shown as ribbons). The ribbon representation of the PI domain is orange. The hydrogen bonds between the side chain of St1Cas9 K1086 and the nucleobase of dG4 is shown as a dashed line. (C-D) The PI domains of St1Cas9 and SaCas9 (PDB: 5CZZ, grey ribbon) are superimposed. In (C), the St1Cas9 Q1084 and SaCas9 R1015 occupy the same position relative to the PAM (dA3). The St1Cas9 E1057 and SaCas9 E993 occupy the same position relative to St1Cas9 Q1084 and SaCas9 R1015, respectively. In (D), St1Cas9 T1048 and M1049 (substituted for N1048 and D1049 in some variants), superimpose onto SaCas9 N985 and N986 that specifies purines in positions 4 and 5 of the PAM. (See also Supplemental Fig. S3).

Figure 3. Broadening the targeting scope of base editors using St1Cas9 variants. (A) K562 cells were transiently transfected with single vector constructs driving expression of St1BE4max LMD9 its sgRNA. Genomic DNA was harvested 3 days later, and quantification of base editing was performed on PCR amplified target sites using EditR. The target sequence was defined as the 20 bases upstream of the PAM and numbered in decreasing order from the PAM. Sequence of the guides and related PAMs are shown with target cytosine highlighted in blue. An expression vector encoding EGFP (-) was used as a negative control. (B-D) Same as (A) but using St1BE4max LMG18311, CNRZ1066 and TH1477 chimeric proteins. (E) Same as (A) but using St1ABEmax LMD9. Target adenines highlighted in red. Most sgRNAs were tested at least twice, only one experiment is shown. (See also Supplemental Fig. S5).

Figure 4. *In vivo* genome editing using St1Cas9. (A) The tyrosine degradation pathway and associated inborn errors of metabolism (IEM). (B) Experimental design. Neonatal (2 days old) *Fah*$^{-/-}$ mice were injected with AAV8-St1Cas9 or saline into the retro-orbital sinus, weaned at 21 days, and NTBC was removed at 30 days of age. Mice off NTBC were killed when they lost 20% of their body weight. (C) Schematic representation of the AAV-St1Cas9 v3 vector. Annotated are the liver-specific promoter (LP1b) promoter, synthetic polyadenylation sequence (SpA) and hU6 promoter. Arrows indicate the direction of transcriptional unit. (D) Neonatal *Fah*$^{-/-}$ mice were injected with either 5 x 10^{10} or 1 x 10^{11} vector genomes (vg) of AAV8-St1Cas9 v3 targeting *Hpd* exon 13 and killed 28 days following injection or kept alive for phenotypic and metabolic studies for 4 months post NTBC removal. Genomic DNA was extracted from whole liver samples and the Surveyor assay was used to determine the frequency of indels. Each dot represents a different mouse. A mouse injected with saline (-) was used as a negative control. (E) SUAC levels in urine from treated mice were determined 15 days (short term) or 4 months (long term) following NTBC removal. Samples were collected from the indicated treatment groups over a 24 hours period using metabolic cages. Number of mice per group/metabolic cage (n) and AAV doses (vg) is indicated. SUAC levels are undetectable in C57BL/6N (wild-type) mice. (F-H) Survival analysis, body weight, and glycemia following NTBC removal in treated mice. Body weight was measured daily and glycemia was monitored in non-fasted mice. Solid lines designate the mean and error bars are represented by shaded areas and denote s.e.m. (See also Supplemental Fig. S6).

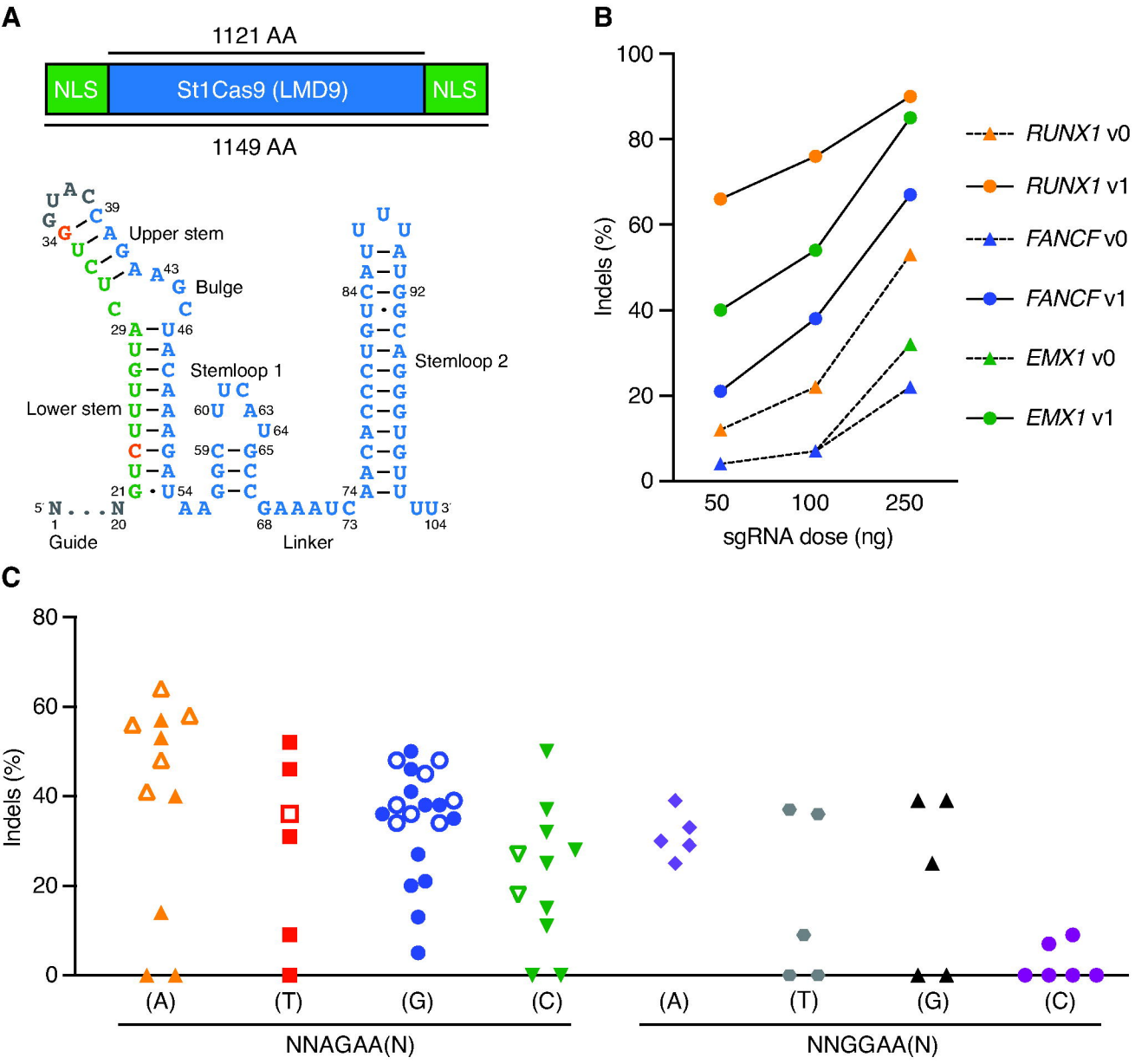

Figure 1
Agudelo et al.

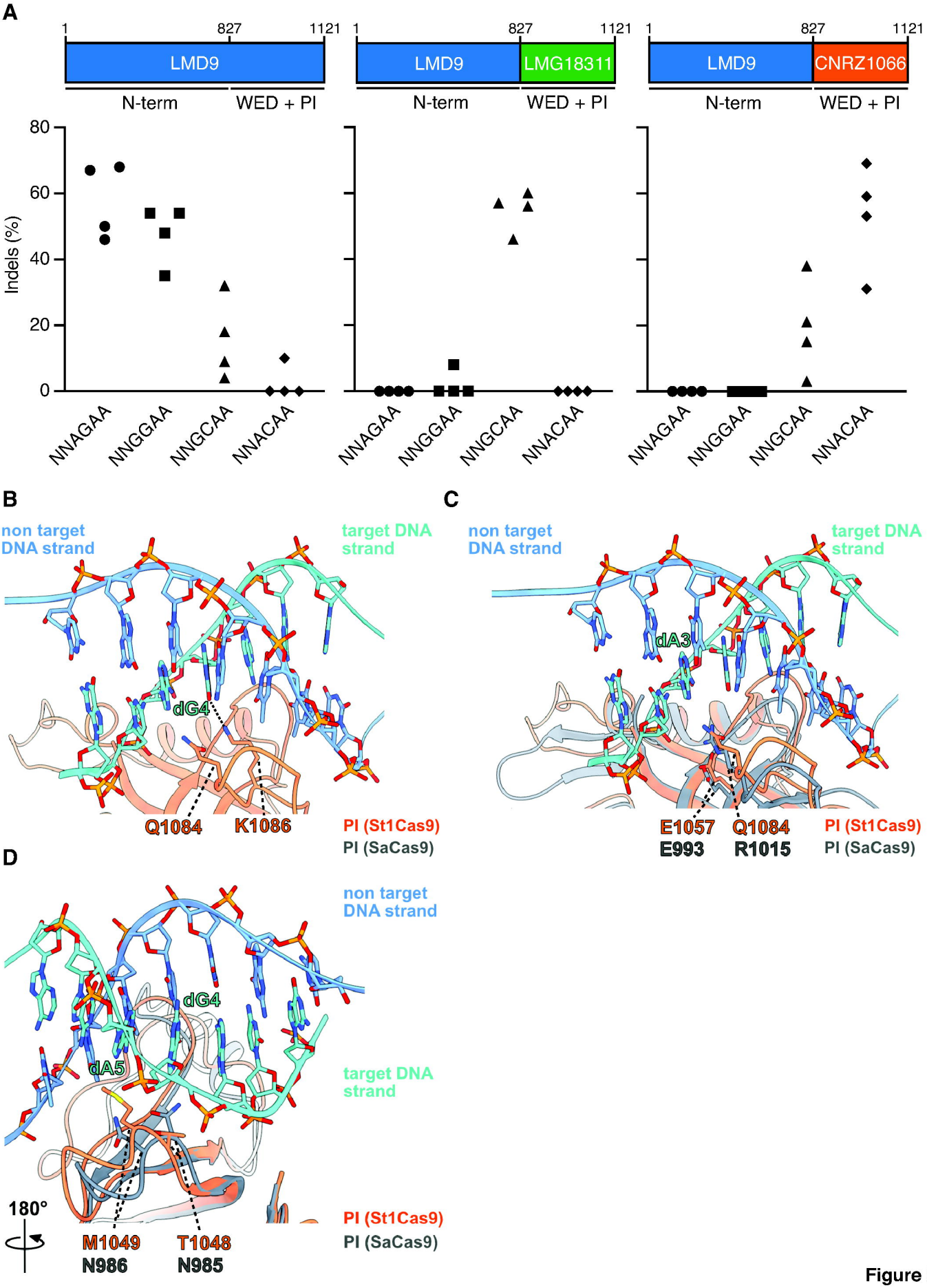

Figure 2
Agudelo et al.

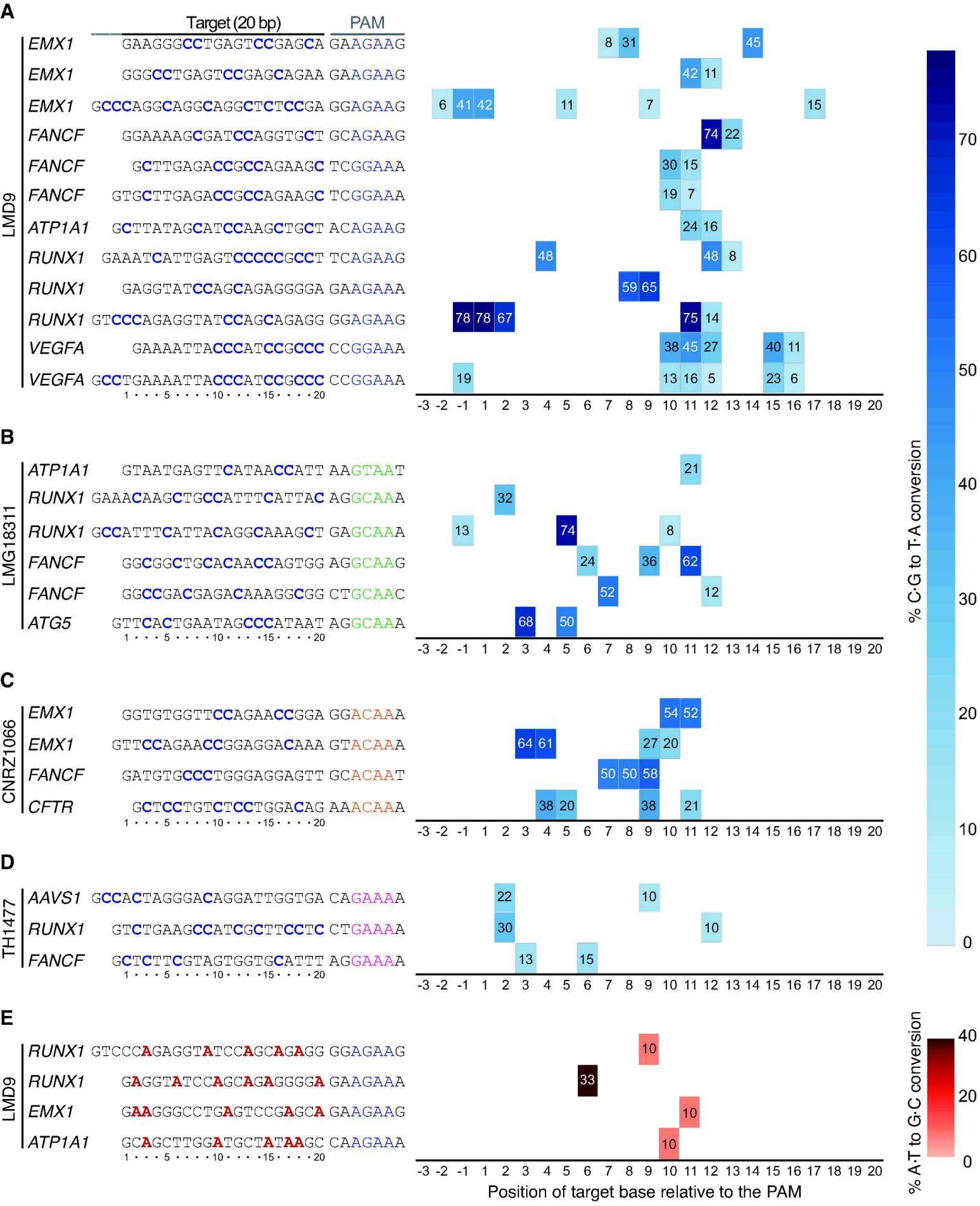

Figure 3
Agudelo et al.

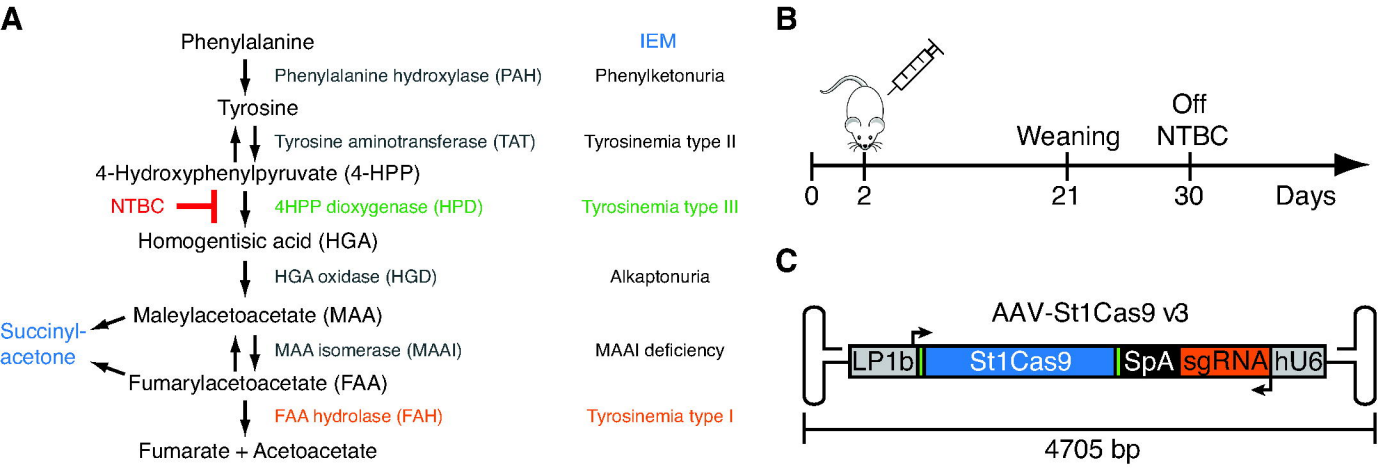

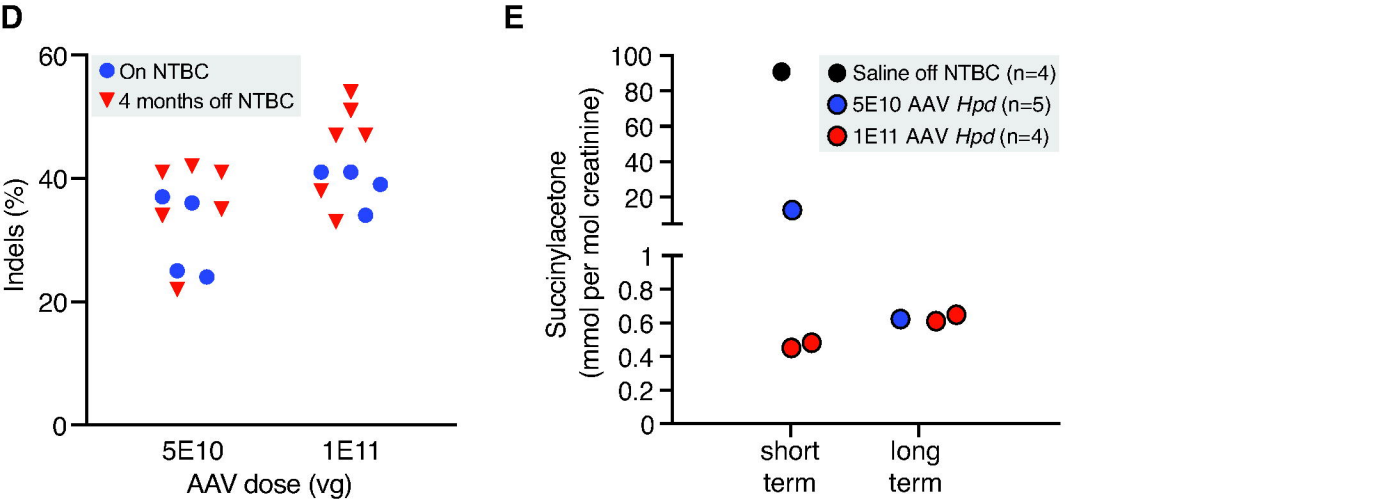

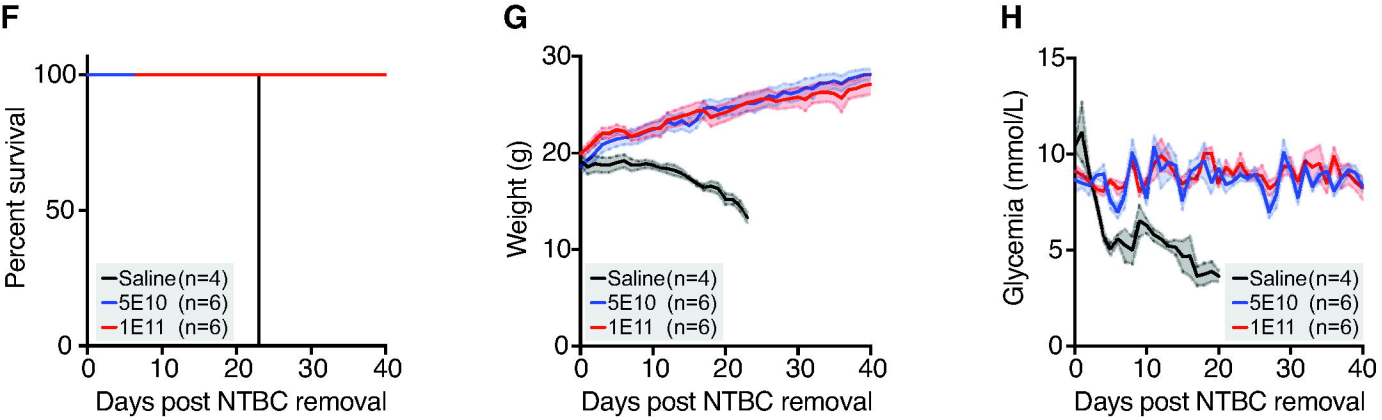

Figure 4
Agudelo et al.